Altered Corneal Epithelial Dendritic Cell Morphology and Phenotype Following Acute Exposure to Hyperosmolar Saline

Kirthana Senthil, Haihan Jiao, Laura E. Downie, and Holly R. Chinnery

Department of Optometry and Vision Sciences, The University of Melbourne, Parkville, Victoria, Australia

Correspondence: Holly R. Chinnery, Department of Optometry and Vision Sciences, The University of Melbourne, 200 Berkeley Street, Carlton, 3053, Australia;
holly.chinnery@unimelb.edu.au.

LED and HRC should be considered joint senior authors.

PURPOSE. The purpose of this study was to assess the morphological and phenotypic responses of corneal epithelial dendritic cells (DCs) to acute topical hyperosmolar stress, given a pathogenic role for tear hyperosmolarity in dry eye disease (DED).

METHODS. C57BL/6J mice were anesthetized and received 350 mOsm/L (physiological; $n = 5$ mice), 450 mOsm/L ($n = 6$), or 600 mOsm/L ($n = 6$) saline on a randomly assigned eye. Corneas were harvested 2 hours later. Immunofluorescent staining was performed using CD45, CD86, and CD68 antibodies to investigate DC morphology (density, viability, field area, circularity, and dendritic complexity) and immunological phenotype. Flow cytometry was used to confirm CD86 and CD68 expression in CD11c$^+$ DCs, using C57BL/6J mice that received topical applications of 350 mOsm/L, 450 mOsm/L, or 600 mOsm/L ($n = 5$ per group) bilaterally for 2 hours.

RESULTS. Following exposure to 450 mOsm/L topical saline for 2 hours, DCs in the central and peripheral cornea were larger (field area: $P_{central} = 0.005$, $P_{peripheral} = 0.037$; circularity: $P_{central} = 0.026$, and $P_{peripheral} = 0.013$) and had higher expression of CD86 compared with 350 mOsm/L controls (immunofluorescence: $P < 0.0001$; flow cytometry: $P = 0.0058$). After application of 600 mOsm/L saline, DC morphology was unchanged, although the percentage of fragmented DCs, and phenotypic expression of CD86 (immunofluorescence: $P < 0.0001$; and flow cytometry: $P = 0.003$) and CD68 (immunofluorescence: $P = 0.024$) were higher compared to 350 mOsm/L controls.

CONCLUSIONS. Short-term exposure to mild hyperosmolar saline (450 mOsm/L) induced morphological and phenotypic maturation in corneal epithelial DCs. More severe hyperosmolar insult (600 mOsm/L) for 2 hours appeared toxic to these cells. These data suggest that hyperosmolar conditions activate corneal DCs, which may have implications for understanding DC activation in DED.

Keywords: cornea, dendritic cell, hyperosmolarity, ocular surface, dry eye, morphology, maturation

D ry eye disease (DED) is a highly prevalent ocular surface disease, estimated to affect about 10% of adults globally.[1] DED has been shown to involve chronic ocular surface inflammation.[2] Common symptoms include sensations of ocular grittiness, conjunctival redness, blurred vision, and eye pain.

Tear hyperosmolarity is common to all DED subtypes and severities,[2,3] with a tear osmolarity ≥ 316 mOsm/L being a sensitive and specific clinical diagnostic marker for DED.[4] Clinically, chronic tear hyperosmolarity has been linked to reduced tear stability[5] and increased tear levels of the pro-inflammatory cytokine interferon-gamma.[6] In mice, recurrent topical application of hyperosmolar solutions (i.e. 3000 mOsm/L) is pro-inflammatory to the mouse conjunctiva, increasing epithelial expression of nuclear factor kappa-B, and priming T cells to promote the development of aqueous-deficient DED.[7] Acute (<10 minute) exposure to mild hyperosmolar stress (<500 mOsm/L) is sufficient to trigger DED-like toxicity[8,9] and release of pro-inflammatory

interleukin-6[9] in *in vitro* assays of human corneal epithelial cells. Thus, although mild, acute hyperosmolar stress can mimic the osmotic insult of DED to the corneal epithelium in an acute experimental setting,[2] it is unknown whether this tear film perturbance can also modulate resident corneal epithelial immune cells *in vivo*. To address this, we evaluated the response of corneal epithelial dendritic cells (DCs) to topical mild hyperosmolar stimuli.

Anatomically, corneal DCs are optimally located to respond to tear hyperosmolarity; they are the predominant immune cell population in the epithelium and have projections that extend up to the tear-epithelial interface[10,11] while interacting with osmosensory nerves.[12–14] Epithelial DCs are also recognized as a clinical marker of corneal inflammation. Using *in vivo* confocal microscopy (IVCM), corneal epithelial DCs have been observed to increase in density[15–19] and change morphology[16,20–23] in clinical and preclinical conditions with corneal inflammation. Changes in both DC density[24–26] and morphology[26,27] have been observed in

patients with DED. However, the specific contribution of hyperosmolar stress to these changes has not been reported.

The aim of the present study was to examine whether corneal epithelial DCs alter in density, morphology, and/or phenotype in response to acute topical hyperosmolarity in vivo. Using immunofluorescent microscopy and flow cytometry, we observed early morphological and phenotypic responses to mild and severe hyperosmolar stress. Our findings support a role for tear hyperosmolarity in modulating corneal immune cell responses.

MATERIALS AND METHODS

Animals

Female C57BL/6J mice (8–12 weeks old), purchased from the Animal Resources Centre (Canning Vale, WA, Australia), were used in accordance with the ARVO Statement for the Use of Animals in Ophthalmic and Vision Research. All procedures received ethics approval from the Florey Institute of Neuroscience and Mental Health animal ethics committee.

Formulation of Saline Solutions

The iso-osmolar (350 mOsm/L) and hyper-osmolar (450 and 600 mOsm/L) saline solutions were formulated by diluting sodium chloride solution (HyperSal 6% hypertonic saline solution; Briemar Nominees Pty Ltd; Royal Children's Hospital Pharmacy, VIC, Australia) in sterile saline (Pfizer Sodium Chloride 0.9% for Injection BP; Pfizer Australia, NSW, Australia). Osmolarity was confirmed prior to topical application based on the average at least two measurements using a freezing point osmometer (Osmette III; Precision Systems, Natick, MA, USA), at room temperature.

Topical Application of Solutions in Anesthetized Mice

C57BL/6J mice were anesthetized with an intraperitoneal injection of ketamine (80 mg/kg) and xylazine (10 mg/kg) and placed in cages, warmed by a heat pad. In experiment A, animals received an 8 µL topical drop of 450 (n = 6 mice) or 600 mOsm/L (n = 6) hyperosmolar saline on a randomly assigned eye. The contralateral eyes, and both eyes in the control group (n = 3), received 350 mOsm/L saline topical drops, as an iso-osmotic stimulus based on previous tear osmolarity measurements in healthy mouse populations.[28,29] One hour into the exposure period, all animals received an additional eye drop of the same tonicity, to compensate for potential evaporation of the applied bolus. All animals were euthanized 2 hours later with an overdose of sodium pentobarbitol (Lethalbarb 150 mg/kg).

To determine whether general anesthesia and the topical applications could have altered corneal DCs in experiment A, a second experiment (experiment B) was conducted comparing untreated C57BL/6J mice (naïve; n = 3) to mice that were treated with 350 mOsm/L saline (n = 3) and unadjusted saline (vehicle; ~280 mOsm/L; n = 3). Similar to experiment A, mice in the 350 mOsm/L and vehicle groups were anesthetized and received an 8 µL topical application of 350 mOsm/L saline or unadjusted sterile saline on contralateral eyes. These mice were euthanized 2 hours later. Mice in the naïve group were euthanized immediately, without anesthesia or topical treatment.
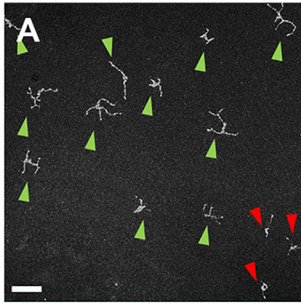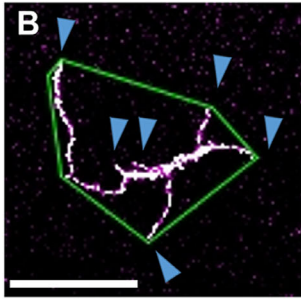
Corneal Immunofluorescent Staining

Mouse eyes were fixed in 4% paraformaldehyde (PFA) for 2 hours at 4°C, after which corneas were dissected and processed for whole-mount immunostaining. Corneas were incubated in 20 mM EDTA at 37°C for 1 hour, then blocked in 1× PBS containing 3% BSA and 0.3% Triton X-100. For morphological analyses, tissues were incubated in primary antibodies against CD45 (1:500; rat anti-mouse CD45; BD Biosciences, Franklin Lakes, NJ, USA; Cat #550539). To assess DC activation, tissues were incubated in primary antibodies against CD86 (1:300; rat anti-mouse CD86; Invitrogen, Eugene, OR, USA; Cat #14-0862-81) or CD68 (1:300; rat anti-mouse CD68; AbD Serotec, Raleigh, NC, USA; Cat #MCA1957), and counterstained with Iba1 (1:300; rabbit anti-mouse Iba1; FUJIFILM Wako, Osaka, Japan; Cat #019-19741) as an equivalent[30] marker to CD45 to identify DCs in the corneal epithelium that is raised in a different species to the rat CD86 and CD68 antibodies. All primary antibodies were mixed in a formulation of 50% 1× PBS + 0.1% Triton X-100 and 20% 1× PBS + 3% BSA + 0.3% TritonX-100, and incubated overnight at 4°C. The samples were then incubated in PBS containing goat anti-rat Alexa Fluor 488 (1:500; Invitrogen; Cat #A11006) and goat anti-rabbit 647 (1:500; Invitrogen; Cat #A21244) secondary antibodies along with Hoechst (1:1000; Hoechst; Sigma-Aldrich, St. Louis, MO, USA; Cat #14533) for 2 hours at room temperature, then cover-slipped using low fade mounting medium.

Image Acquisition

Corneas stained with CD45 were imaged on the Leica SP8 Confocal Inverted Laser Scanning Microscope (Leica Microsystems) using a 20× objective. Based on the reported topographic differences in mouse DC morphology during homeostasis and inflammation,[30] both the central and peripheral cornea were analyzed separately. For morphological analysis, 2 epithelial z-stacks were captured in the central-most 1/3 of each corneal flatmount (to define "central DCs"), and 3 epithelial z-stacks were captured in the peripheral 2/3 of the corneal flatmount (to define "peripheral DCs"), excluding the limbus (Supplementary Fig. S1a). Hoechst staining was used to define the z-boundaries of the epithelium. Higher-resolution z-stacks were also collected using a 63× objective to compare nuclear morphology in DCs. To examine DC immunophenotype, two epithelial z-stacks were taken from the central and peripheral regions of CD86- and CD68-stained tissue samples (see Supplementary Fig. S1b) using a 40× objective (290 × 290 µm field; 512 × 512 pixels per frame). All imaging settings (i.e. laser power, gain and offset, image format, and 1 µm step size) were consistent for all samples.

Corneal Dendritic Cell Morphological Analyses

Morphological features of corneal epithelial DCs were analyzed using two-dimensional maximum projection images on ImageJ software (version 1.52d; National Institute of Health, USA) by a masked observer. CD45^{+} DCs were selected for morphological analysis based on their characteristic dendritiform morphology, and location within the epithelium[31], and other non-dendritiform immune cells were excluded. DC density and viability were then manually counted and averaged between two 20× images (581 × 581 µm field) from the central and peripheral cornea.

Parameter	Description	Method
Density (cells/mm²)	Average number of CD45+ dendritiform cells between 2 images in the central or peripheral cornea per animal. Both viable (green arrowhead) and non-viable (red arrowhead) cells were included. Rarely-occurring round, non-dendritic cells were excluded.	Z-project + manual counting
Viability (%)	Percentage of the total number of dendritiform CD45+ cells (viable and non-viable) that appear fragmented (red arrowhead).	Z-project + manual counting
Dendritic Complexity (Dendritic tips/cell)	Number of dendritic tips per cell (blue arrowheads).	Z-project + manual counting
Cell area (µm²)	Area of the CD45+ DC (magenta) above the manually chosen threshold (white) within the polygon border (green).	Z-project + Polygon tool + Threshold + Measure (Area)
Field area (µm²)	Total epithelial area encompassed per DC, as defined by the Polygon border (green).	Z-project + Polygon tool + Threshold + Measure (Area & %Area) + manual calculation
Circularity (circularity index)	The circularity of the DC above threshold (white) relative to the Polygon outline and standardized to a value between 0 and 1.	Z-project + Polygon tool + Threshold + Measure (Shape descriptors)

FIGURE 1. **Methods for quantifying two-dimensional corneal dendritic cell (DC) morphology, including relevant parameter definitions.** Representative 20× confocal maximum projection z-stack image (**A**) showing how DC density and viability were quantified with the identification of viable dendritiform CD45-positive cells (*green arrowheads*) and nonviable dendritiform CD45-positive cells (*red arrowheads*). Representative higher-magnification confocal maximum projection z-stack (**B**) showing key quantification features, including tracing the DC perimeter with the ImageJ Polygon tool (*green border*), the Threshold tool (*white*) applied over the CD45-labeled DC (*magenta*), and the location of dendritic tips (*blue arrowhead*), as used to quantify DC complexity, cell area, field area, and circularity. Scale bar for all images is 50 µm.

Nonviable DCs were identified using basic pathological signs of membrane lysis as a marker for cell death.[24–26]

Two-dimensional DC parameters of dendritic complexity, cell area, field area, and circularity were also calculated, as previously described in human[27] and murine[30,32] DC morphometry studies (see Fig. 1 for further detail). The Polygon tool was used to define the borders of each DC at each dendritic tip, after which the DC morphology was outlined by a fluorescence intensity threshold (manually set for each image and each fluorophore) and the "Measure" function was applied. Values were calculated separately for the central and peripheral cornea and each DC is presented as an independent unit.[7,19]

Corneal Dendritic Cell Immunophenotypic Analysis

DC phenotype was assessed using the activation markers, CD86 and CD68, which are associated with corneal inflammation.[31,33–35] CD86 is a costimulatory cell surface molecule that is upregulated on corneal DCs following inflammatory stimulation.[36] CD68 is an endosomal/lysosomal glycoprotein that is typically used to identify macrophages but is upregulated in DCs exposed to hyperosmolar stress.[37,38] To quantify CD86 and CD68 expression within DCs, a masked observer created a binary maximum projection of the 40× epithelial z-stacks based on Iba1 staining only (manually adjusted threshold). Whole individual cells were selected with the "Rectangle" tool and a mask was created based on the Iba1-stained outline to exclude all background fluorescence. CD86 expression was measured within each DC mask using the "Mean Gray Value" tool. The number and percent-age area of CD68^{high} particles were quantified in each cell mask with additional thresholding of the CD68-labeled channel (set equally in all groups) and the "Analyze Particles" tool - similar to the protocol described by Cope et al. (2018).[39] Due to low cell numbers in the central cornea, DCs in the peripheral and central regions were pooled together as a single "corneal epithelial DC" population and presented as independent samples.[7,19]

Flow Cytometry

Flow cytometry was performed to assess the immunophenotype of corneal epithelial DCs after the 2-hour osmotic stressor. Anaesthetized C57BL/6J mice received topical application of 350, 450, or 600 mOsm/L saline ($n = 5$ mice per experimental group) for 2 hours on both eyes. Corneas were then analyzed using the same flow cytometry protocol described by Jiao et al.[32] Both corneas from each mouse (total of 10 corneas per treatment, split into 4 replicates) were carefully dissected to remove the iris and limbus and digested in Dulbecco's modified Eagle's medium F12 (DMEM F-12, 0.1 mM Ca²⁺) containing 2 mg/mL Collagenase-D and 0.5 mg/mL DNAase-1 (Roche, Indianapolis, IN) for 40 minutes at 37°C. Single cell suspensions were then filtered and labeled with conjugated primary antibodies against CD45 (CD45-PE; BioLegend, San Diego, CA, USA; Cat #103105 1:200), CD11c (CD11c-PeCy7; Invitrogen; Cat #25011482; 1:200) and either CD86 (CD86-APC; Invitrogen; Cat #17086281; 1:200) or CD68 (CD68-APC; BioLegend; Cat #137007; 1:200) for 30 minutes on ice. Unstained controls omitting the above antibodies were also included. All samples were counterstained with DAPI (1:100) and then assessed on CytoFlex S Flow Cytometer (Beckman Coulter)
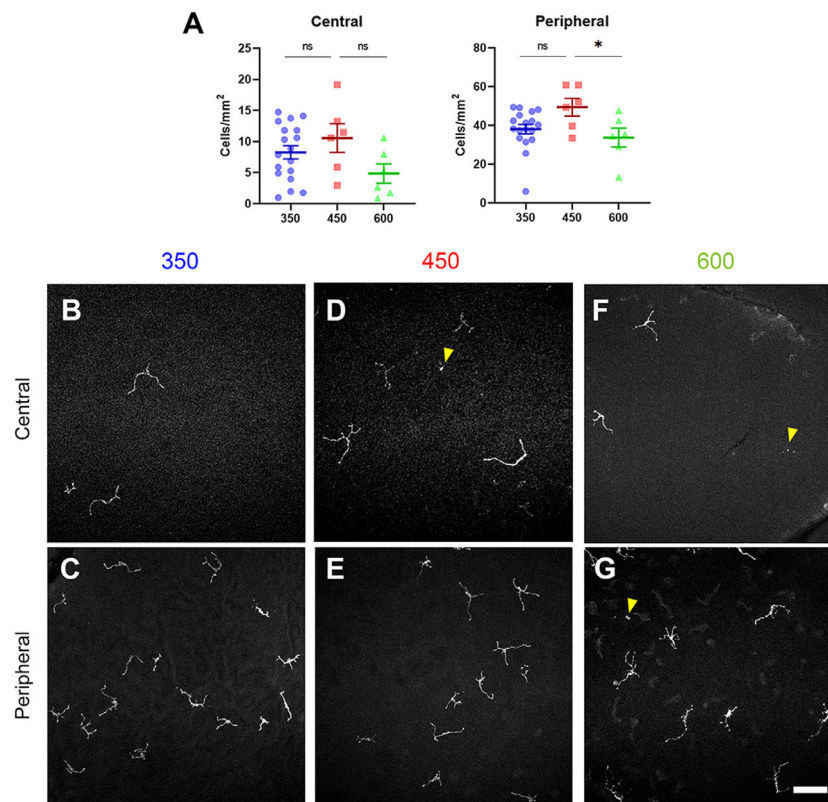
FIGURE 2. **Dendritic cell (DC) density in the central and peripheral cornea.** Plots (**A**) and representative images (**B–G**) of DCs in the central (**B, D, F**) and peripheral cornea (**C, E, G**) show no differences between eyes that received topical applications of 350 mOsm/L (**B, C**), 450 mOsm/L (**D, E**) and 600 mOsm/L (**F, G**) saline for 2 hours. DC density was quantified based on CD45-positive staining, dendritiform morphology, and location within the epithelial plane of focus. Nonviable cells (*yellow arrowhead*) were included in the counts. Each data point represents the average value taken from three images per cornea. $N = 18$, 6, and 6 corneas in the 350, 450, and 600 mOsm/L groups, respectively. Data are presented as mean ± SEM. Scale bar for all images is 100 µm.

with 30,000 events recorded per sample. FlowJo software (version 10) was used to analyze the data in all groups.

Statistical Analyses

All statistical analyses were performed using GraphPad Prism software (version 8.0.1; GraphPad Software, La Jolla, CA, USA). After confirming data were normally distributed, inter-group comparisons were analyzed using a 1-way ANOVA with Tukey's post hoc test for multiple comparisons. Additionally, data from 350 mOsm/L-treated eyes in experiment A were confirmed to have no contralateral effect using a Student's *t*-test before combining into a single 350 mOsm/L baseline group. Unless otherwise stated, all reported statistics refer to the inter-group comparisons from the Tukey's post hoc test, with data expressed as mean (M) ± SEM. An alpha of 0.05 was adopted for statistical significance. The P values in plots are summarized using; *$P < 0.05$, **$P < 0.01$, ***$P < 0.001$, and ****$P < 0.0001$.

RESULTS

Corneal Epithelial DC Density

CD45 staining allows visualization of the resident DC population in the corneal epithelium.[31,32,40,41] Mean corneal DC density across all osmotic groups ranged from 4 to 11 cells/mm² centrally, to 33 to 50 cells/mm² peripherally. As an increase in epithelial DC density is an indicator of corneal inflammation in clinical[42] and laboratory[31,36] settings, this parameter was quantified in corneas exposed to different osmotic stimuli. After 2 hours of topical 450 mOsm/L or 600 mOsm/L stress, corneal epithelial DC density did not differ from the iso-osmotic 350 mOsm/L condition, in the central ($M_{350} = 8.27 \pm 1.07$ cells/mm², $M_{450} = 10.55 \pm 2.32$ cells/mm², $M_{600} = 4.85 \pm 1.56$ cells/mm², $p_{350 v 450} = 0.55$, $p_{350 v 600} = 0.28$) or peripheral cornea ($M_{350} = 38.07 \pm 2.44$ cells/mm², $M_{450} = 49.42 \pm 4.56$ cells/mm², $M_{600} = 33.69 \pm 4.87$ cells/mm², $p_{350 v 450} = 0.08$, $p_{350 v 600} = 0.66$; Fig. 2). DC density was also similar in naïve mice and those that received 350 mOsm/L treatment or vehicle treatment, in central ($M_{naive} = 5.73 \pm 2.09$ vs. $M_{350} = 10.81 \pm 3.89$ cells/mm², $P = 0.56$) and peripheral regions ($M_{naive} = 28.34 \pm 3.98$ vs. $M_{350} = 41.11 \pm 4.90$ cells/mm², $P = 0.26$; see Supplementary Fig. S3a).

Corneal Epithelial DC Morphology

In response to topical hyperosmolar stress, corneal DCs showed morphological differences irrespective of eccentricity. DCs in mice treated with 450 mOsm/L saline had a more enlarged morphology than mice treated with 350 mOsm/L, with a larger field area (central: $M_{350} = 1670 \pm 89.94$ vs. $M_{450} = 2233 \pm 187.5$ µm², $P = 0.005$; peripheral: $M_{350} = 1552 \pm 36.5$ vs. $M_{450} = 1723 \pm 61.98$ µm², $P = 0.037$; Fig. 3a) and lower circularity (central: $M_{350} = 0.072 \pm 0.004$
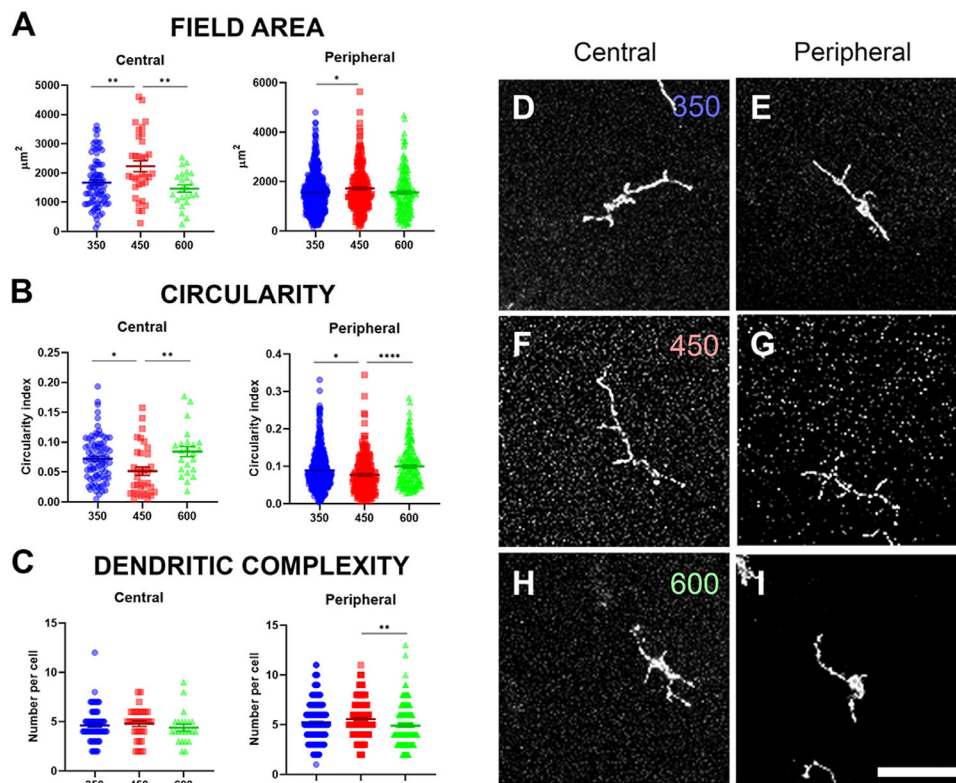
FIGURE 3. **Corneal dendritic cell (DC) morphology.** Field area (**A**), circularity (**B**), and dendritic complexity (**C**) of CD45-labeled DCs were different in the central and peripheral cornea following 2-hour, in vivo topical exposure to 350 mOsm/L, 450 mOsm/L, and 600 mOsm/L saline. DCs showed eccentricity-dependent changes to topical hyperosmolarity, with central DCs having a higher field area and lower circularity after 450 mOsm/L treatment relative to those treated with 350 mOsm/L. In peripheral corneal DCs, there was only a reduction in circularity after 450 mOsm/L treatment compared to 350 mOsm/L controls. Higher-magnification representative confocal maximum z-stack projections (CD45-stained) showing DC morphology after topical application of 350 mOsm/L (**D, E**), 450 mOsm/L (**F, G**) and 600 mOsm/L (**H, I**) in the central (**D, F, H**) and peripheral (**E, G, I**) cornea. Each data point represents a single DC. N (central) = 84, 34, and 23 cells, and N (peripheral) = 491, 213, and 156 cells in the 350, 450, and 600 mOsm/L groups, respectively. Data are presented as mean ± SEM. Asterisks denote statistical significance between groups (*$P < 0.05$, **$P < 0.01$, ****$P < 0.0001$). Scale bar for all images is 50 µm.

vs. $M_{450} = 0.051 ± 0.007$, $P = 0.026$; peripheral: $M_{350} = 0.089 ± 0.002$ vs. $M_{450} = 0.077 ± 0.003$, $P = 0.013$; Fig. 3b). Meanwhile, cell area (central: $M_{350} = 154.8 ± 7.42$ vs. $M_{450} = 144.4 ± 16.40$ µm², $P = 0.78$; peripheral: $M_{350} = 174.6 ± 3.32$ vs. $M_{450} = 196.9 ± 6.023$ µm², $P = 0.13$) and dendritic complexity remained similar (central: $M_{350} = 4.62 ± 0.18$ tips vs. $M_{450} = 4.79 ± 0.27$ tips, $P = 0.86$; peripheral: $M_{350} = 5.25 ± 0.086$ vs. $M_{450} = 5.56 ± 0.12$ tips, $P = 0.11$; Fig. 3c). Together, these findings suggest that the change in DC field area and circularity may result from cytoplasmic extension, rather than an altered dendrite configuration. Following a higher (600 mOsm/L) hyperosmolar stress, there were no overt changes to DC morphology. Both central and peripheral DCs exposed to 600 mOsm/L had a similar morphology to the 350 mOsm/L controls with respect to field area (central: $M_{600} = 1466 ± 126.6$ µm², $P_{350 v 600} = 0.57$; peripheral: $M_{600} = 1557 ± 69.88$ µm², $P_{350 v 600} = 0.99$; see Fig. 3a), circularity (central: $M_{600} = 0.084 ± 0.0084$, $P_{350 v 600} = 0.40$; peripheral: $M_{600} = 0.1 ± 0.0043$, $P_{350 v 600} = 0.058$; see Fig. 3b) and dendritic complexity (central: $M_{600} = 4.39 ± 0.34$ tips, $P_{350 v 600} = 0.82$; peripheral: $M_{600} = 4.91 ± 0.16$ tips, $P_{350 v 600} = 0.12$; see Fig. 3c). DCs exposed to 600 mOsm/L saline showed lower viability in the central cornea relative to iso-osmotic controls ($M_{350} = 90.67 ± 2.91\%$ vs. $M_{600} = 63.19 ± 13.28\%$, $P = 0.0062$; see Supplementary Fig. S2), and many cells showed uneven immunohistochem-

ical membrane staining, similar to membrane blebbing in stressed cells. Within these blebbed cells, nuclei appeared to be segmented at multiple points, similar to nuclear fragmentation described in apoptotic cells[43] (see Supplementary Figs. S2g, S2h).

To confirm that anesthesia and topical saline application did not alter DC parameters, corneas were treated with iso-osmotic saline (vehicle) or 350 mOsm/L saline and compared to naïve, un-anesthetized mouse corneas. In mice that were anesthetized and received either vehicle or 350 mOsm/L saline, DCs throughout the central and peripheral cornea had a smaller morphology and lower field area in both the central ($M_{naïve} = 2097 ± 265.0$ µm², $M_{vehicle} = 1457 ± 104.1$ µm², $M_{350} = 1340 ± 104.2$ µm², $P_{naïve v vehicle} = 0.01$, $P_{naïve v 350} = 0.001$) and peripheral regions ($M_{naïve} = 2605 ± 88.78$ µm², $M_{vehicle} = 1828 ± 78.98$ µm², $M_{350} = 2068 ± 64.95$ µm², $P_{naïve v vehicle} < 0.0001$, $P_{naïve v 350} < 0.0001$; see Supplementary Fig. S4a).

Corneal Epithelial DC Phenotype

We next assessed the immunophenotypes of DCs in both confocal microscopy and flow cytometry using CD86 and CD68. Confocal microscopy was the primary method in which phenotypic analysis was conducted so that corneal epithelial DCs could be examined in isolation of other
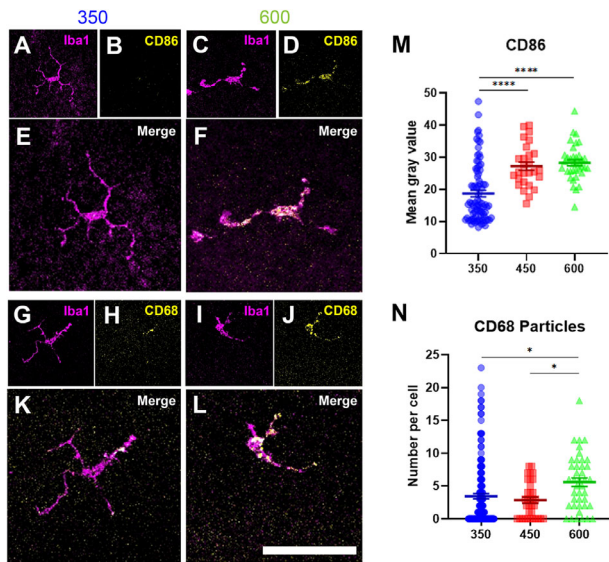
FIGURE 4. **Immunofluorescence analysis of corneal epithelial dendritic cell (DC) phenotype.** Increased expression of CD86 (**A–F**) and CD68 (**G–L**) in Iba1-labeled DCs exposed to 600 mOsm/L compared to 350 mOsm/L saline, which is also quantitatively presented as higher fluorescence intensity staining with CD86 (**M**) and a higher number of CD68 particles (**N**). Eyes treated with 450 mOsm/L saline showed a higher intensity of CD86 staining within Iba1-labeled DCs compared to the 350 mOsm/L saline condition. Data points represent individual DCs in both the central and peripheral cornea. N (CD86) = 82, 27, and 36 cells, and N (CD68) = 162, 34, and 41 cells in the 350, 450, and 600 mOsm/L groups for CD86 and CD68 analysis, respectively. Data are presented as mean ± SEM. Asterisks denote statistical significance between groups (*$P < 0.05$, ****$P < 0.0001$). Scale bars for all images is 50 µm.

similar cell-types like stromal DCs *in situ* – a feature that is not possible with flow cytometry. Eccentricity-based differences were also not examined; DCs in the central and peripheral cornea were concatenated to compensate for lower cell numbers in the 290 × 290 µm field of view.

Throughout the naïve corneal epithelium, there was very low CD86 and CD68 expression within Iba1^{+} DCs,[30] although some CD86^{high} and CD68^{high} DCs were present (see Supplementary Fig. S5). Despite observed morphological retraction (see Supplementary Fig. S4a), DCs in anesthetized mouse corneas that were treated with vehicle (iso-osmotic 350 mOsm/L saline), showed equivalent CD86 fluorescence intensity and CD68 particles to naïve mice (CD86: $M_{naive} = 28.73 \pm 0.87$ intensity units vs. $M_{350} = 27.75 \pm 0.77$ intensity units, $P = 0.69$; CD68: $M_{naive} = 5.08 \pm 0.94$ particles vs. $M_{350} = 3.62 \pm 0.43$ particles, $P = 0.23$; see Supplementary Fig. S5), indicating retention of physiological steady-state.

Following topical 450 mOsm/L stress, DCs had higher CD86 staining compared to 350 mOsm/L controls ($M_{350} = 18.76 \pm 1.02$ intensity units vs. $M_{450} = 27.27 \pm 1.28$ intensity units, $p_{350 \text{ v } 450} < 0.0001$; Fig. 4) but there was no inter-condition difference in CD68 staining ($M_{350} = 3.44 \pm 0.40$ particles vs. $M_{450} = 2.85 \pm 0.46$ particles, $P = 0.78$). In response to 600 mOsm/L, corneal DCs showed elevations in CD86 ($M_{600} = 28.34 \pm 0.94$ intensity units, $P_{350 \text{ v } 600} < 0.0001$) and CD68 staining ($M_{600} = 3.39 \pm 0.54$ particles, $P_{350 \text{ v } 600} = 0.032$).

We next compared the activation status of all CD45^{+}CD11c^{+} corneal DCs following hyperosmolar stress, using flow cytometry as a more sensitive measure of immunophenotype. Using the gating strategy (Fig. 5a), we found a significantly higher proportion of CD86^{+}CD45^{+}CD11c^{+} DCs in the 450 mOsm/L ($M_{350} = 18.38 \pm 1.53\%$ vs. $M_{450} = 32.53 \pm 1.72\%$, $P_{350 \text{ v } 450} = 0.006$; Fig. 5c) and 600 mOsm/L groups relative to the 350 mOsm/L group ($M_{600} = 40.38 \pm 3.41\%$, $P_{350 \text{ v } 600} = 0.0003$; Fig. 5c). However, the proportion of CD68^{+} DCs was unchanged ($M_{350} = 10.57 \pm 1.89\%$ vs. $M_{450} = 15.23 \pm 1.38\%$ vs. $M_{600} = 15.73 \pm 3.46\%$, $P_{350 \text{ v } 450} = 0.47$, $P_{350 \text{ v } 600} = 0.36$; Fig. 5d).

DISCUSSION

Corneal epithelial DCs are a key component of innate immunity at the ocular surface and are often considered in terms of their density and topographical distribution in the context of inflammation. However, the morphological and phenotypic responses of corneal epithelial DCs to acute topical hyperosmolar stress have not been previously examined despite the relevance of tear hyperosmolarity to DED pathogenesis.[2,3,44] In this study, we investigated the changes in murine corneal DCs after 2 hours of ocularsurface stimulation with different concentrations of hyperosmotic saline. This experimental regimen intended to mimic tear hyperosmolar stresses considered to induce corneal inflammation in DED.[2] Congruent with previous studies of DC maturation in patients with DED[26,27] and murine models of DED,[45,46] in our study acute hyperosmolar stress was associated with distinct morphological and phenotypic changes to DCs.

DCs are dynamic[47] cells; the extension and retraction of their dendrites directly relate to antigen-sampling, cross-presentation, and migration functionalities.[48,49] These properties are advantageous in the steady-state corneal epithelium as long dendritic projections allow efficient antigen-capture over a large epithelial area despite the sparse presence of DCs. In our study, the steady-state cornea was mimicked by topical application of 350 mOsm/L saline, based on the reported tear osmolarity in young healthy mouse populations.[28,29] DCs in mice treated with topical 350 mOsm/L saline were equivalent in density and morphology to previously reported healthy corneal DC populations,[30] validating the use of 350 mOsm/L saline as an iso-osmotic control. DC immunophenotype was also evaluated using conventional and unconventional activation markers, CD86 and CD68, respectively. Although these molecules have been reported to be exclusively expressed by resident immune cells in the corneal stroma of mice during steady-state,[12,33,50] we found low, but similar expression in naïve and 350 mOsm/L-treated corneal epithelial DCs.

Corneal DCs show a variety of stimulus-dependent morphological responses to inflammatory activation, including dynamic extension of existing and new dendrites,[16,27,30] increased probing activity,[47] and retraction of their dendrites to form a spherical morphology.[51] In response to the 450 mOsm/L topical stressor, DCs in our study upregulated CD86, indicating activation, in parallel with an enlarged morphology, increased field area, and reduced circularity. This cytoplasmic extension is commonly referred to as a "maturation" response and has been reported in human corneal DCs during inflammatory conditions, such as diabetes,[20] rheumatoid arthritis,[22] mild cognitive impairment,[52] and allergy,[21] and in murine corneas after sterile epithelial injury and exposure to the toll-like receptor-9 ligand, CpG-ODN.[30] Although most of these studies demonstrate DC maturation in the context of chronic inflammation,
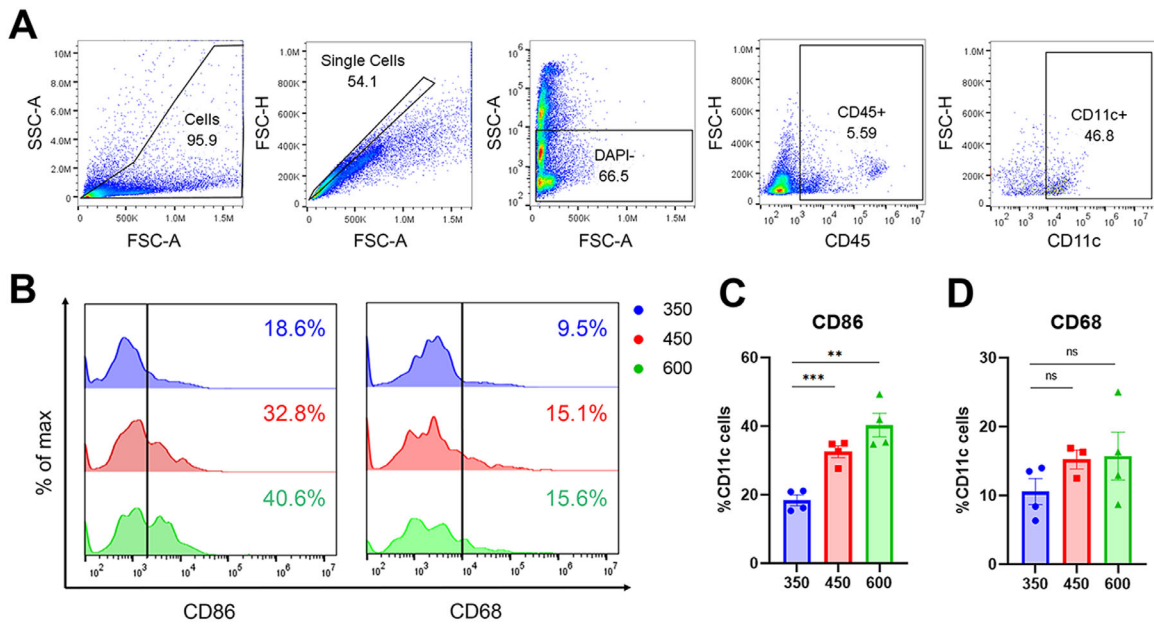
FIGURE 5. **Flow cytometry analysis of corneal dendritic cell (DC) phenotype.** Using a gating strategy (**A**), the CD86+/CD68+ CD45+CD11c+ DCs were isolated and examined for each saline treatment. The modal histograms (**B**) show the CD86 and CD68 staining intensity of the concatenated DC populations in each treatment group, with the bold line delineating the CD86 and CD68 gating threshold. The percentage of CD86+ DCs (**C**) increased in corneas after topical application of 450 mOsm/L and 600 mOsm/L saline compared to 350 mOsm/L saline, whereas CD68+ DCs (**D**) did not differ between groups. Data are presented as mean ± SEM. Asterisks denote statistical significance between groups (**$P < 0.01$, ***$P < 0.001$). ns, not statistically significant.

our findings show that altered morphology is the earliest indicator of DC activation, occurring within 2 hours of hyperosmotic exposure and preceding changes in DC density.

In the present study, topical application of 450 mOsm/L saline was chosen to experimentally model the osmotic insult that occurs in DED. Although DED is a chronic condition characterized by a long-term elevation in tear osmolarity,[44] the TFOS DEWS II report indicates that the condition can be acutely modelled using a 450 mOsm/L stimulus; in vitro studies demonstrate this stressor induces DED-like inflammatory cytokine release, and epithelial cell death in the cornea[8,9] and conjunctiva.[53] This level of hypertonicity is also the lowest osmolarity at which nociceptors show electrical activity in mice,[54] and corneal pain is perceived by humans.[8] Hence, our finding of DC phenotypic and morphological activation in response to ocular surface stimulation with a 450 mOsm/L solution, being a conservative hyperosmotic stressor, confirms the corneal inflammatory potential of relatively modest elevations in tear osmolarity.

The observed DC maturation response to ocular surface hyperosmolarity also closely resembles the increase in DC size, field area, and dendritic complexity reported in DED patients.[26,27] Morphological and phenotypic signs of DC maturation, as reported in our study in response to 450 mOsm/L stress, typically correspond with acute inflammation and upregulation of costimulatory molecules that are critical for antigen presentation.[48] For example, DC maturation was correlated to tear concentrations of interleukin-1β, interleukin-6, and interleukin-7 in patients with bacterial keratitis.[15] Thus, mature DCs likely play a critical role in DED pathogenesis, as supported by the increased presence and T cell stimulation by CD86^{high} DCs in the cervical lymph nodes in mice after 4 days of evaporative (hyperosmolar) stress.[45]

Hyperosmolar stress may also act as a DC primer during DED pathogenesis. Renal DCs and cultured bone marrow-derived DCs both upregulate CD86 and CD68 in response to hyperosmolar stress, although the capacity to stimulate T cells only occurred in the presence of a secondary bacterial stimulus (lipopolysaccharide [LPS]).[37] Similarly, Vega-Ramos et al. reported that DCs lack the capacity to secrete cytokines when activated without an antigen, but remain primed until a secondary antigen is introduced, whereupon there is hypersecretion of inflammatory cytokines.[55] As hyperosmolar stress does not constitute an antigen, by virtue of its inability to be cross-presented to T cells, it is likely that our findings provide evidence for DC priming without induction of the adaptive immune response. Consistent with this hypothesis, T cells derived from the submandibular lymph nodes of mice treated with 3000 mOsm/L saline for 5 days induce a heightened swelling response when injected into a mouse footpad with ovalbumin antigen, and accelerate the impediment to tear production when injected into mice undergoing evaporative stress. Concurrent to this T cell priming, conjunctival DCs augmented their morphology after 5-day treatment of 3000 mOsm/L saline, similar to our findings in the cornea.

DCs did not show morphological changes in response to 600 mOsm/L stress, relative to 350 mOsm/L controls. Instead, there were signs of DC membrane blebbing and fragmentation in the central cornea, suggesting these cells were arrested and potentially undergoing cell death. DCs exposed to 600 mOsm/L saline also exhibited increased activation marker expression, consistent with evidence of starvation-induced apoptosis in cultured DCs.[56] This was a somewhat unexpected result. Although in vitro exposure to a 600 mOsm/L stimulus can induce nociceptor injury[54] and epithelial cell death,[57] a topical drop of 600 mOsm/L saline

induces only mild pain perception in humans[8] and is below the theorized 2000 mOsm/L osmotic level at the epicentre of tear film breakup spots.[58] Many topical ophthalmic hyperosmolar preparations prescribed for treating corneal edema, such as Muro-2% (≈700 mOsm/L[59]) and Muro-5% (≈1700 mOsm/L[59]), are also considered safe, with a low reported incidence of ocular surface pain and corneal damage.[60] To the best of the authors' knowledge, the direct effect of acute hyperosmolar saline exposure on resident corneal DCs has not been reported. Hence, it is interesting that DC toxicity may have been observed in our study given the 600 mOsm/L stimulus was not within a known pathological range in an in vivo setting. The difference in exposure periods may also explain this finding. Mice in our study were exposed to 600 mOsm/L stress for 2 hours, whereas the typical residence time of topical hyperosmolar preparations in humans is considered in the order of a few minutes.[61,62] Irrespective of this difference, our findings have implications for understanding how corneal DC physiology is altered after topical hyperosmolar treatment. Our findings may also be relevant to understanding cumulative alterations to DC physiology in populations with decreased tear stability, such as infrequent blinkers,[63] heavy computer users,[64] and patients with DED.[5]

This study was limited by the use of anesthetized mice. Not only did we detect retraction in the resting morphology of DCs in anesthetized mice, but general anesthesia is reported to disrupt corneal homeostasis by inducing corneal thinning,[65] structural damage[66] and altering tear film biochemistry.[67] Hence, our findings after 2 hours of uninterrupted hyperosmolar stress in anesthetized mice are not completely generalizable to the natural *in vivo* conditions of acute hyperosmolar stress in humans. Further *in vivo* experiments in laboratory and clinical settings are required, with a focus on shorter exposures to hyperosmolar stress.

CONCLUSION

Corneal epithelial DCs undergo morphological and phenotypic changes when exposed to a hypertonic topical stimulus, with a larger and activated morphology in response to mild (450 mOsm/L) stress, and immunophenotypic activation and morphological alterations consistent with reported features of DC death in response to severe (600 mOsm/L) stress. Considering the role of hyperosmolar stress in the pathogenesis of DED, these data support a role for corneal DC activation following the loss of tear homeostasis.

Acknowledgments

All authors have no conflicts to disclose. L.E.D. has received funding from Alcon, Allergan, and Azura Ophthalmics for dry eye research, and consulting income from Seqirus and Medmont, all unrelated to this work.

Author contributions: K.S., L.E.D., and H.R.C. designed and performed experiments and data analysis. H.J. performed experiments. K.S., L.E.D., and H.R.C. drafted the paper. All authors have read, reviewed, and approved the final paper as submitted.

Disclosure: **K. Senthil,** None; **H. Jiao,** None; **L.E. Downie,** None; **H.R. Chinnery,** None

References

1. Stapleton F, Alves M, Bunya VY, et al. TFOS DEWS II Epidemiology Report. *Ocul Surf.* 2017;15(3):334–365.

2. Bron AJ, de Paiva CS, Chauhan SK, et al. TFOS DEWS II pathophysiology report. *Ocul Surf.* 2017;15(3):438–510.

3. Pflugfelder SC, de Paiva CS. The pathophysiology of dry eye disease: what we know and future directions for research. *Ophthalmology.* 2017;124(11S):S4–S13.

4. Lemp MA, Bron AJ, Baudouin C, et al. Tear osmolarity in the diagnosis and management of dry eye disease. *Am J Ophthalmol.* 2011;151(5):792–798.e791.

5. Downie LE. Automated tear film surface quality breakup time as a novel clinical marker for tear hyperosmolarity in dry eye disease. *Invest Ophthalmol Vis Sci.* 2015;56(12):7260–7268.

6. Jackson DC, Zeng W, Wong CY, et al. Tear interferon-gamma as a biomarker for evaporative dry eye disease. *Invest Ophthalmol Vis Sci.* 2016;57(11):4824–4830.

7. Guzmán M, Miglio M, Keitelman I, et al. Transient tear hyperosmolarity disrupts the neuroimmune homeostasis of the ocular surface and facilitates dry eye onset. *Immunology.* 2020;161(2):148–161.

8. Liu H, Begley C, Chen M, et al. A link between tear instability and hyperosmolarity in dry eye. *Invest Ophthalmol Vis Sci.* 2009;50(8):3671–3679.

9. Igarashi T, Fujimoto C, Suzuki H, et al. Short-time exposure of hyperosmolarity triggers interleukin-6 expression in corneal epithelial cells. *Cornea.* 2014;33(12):1342–1347.

10. Lee EJ, Rosenbaum JT, Planck SR. Epifluorescence intravital microscopy of murine corneal dendritic cells. *Invest Ophthalmol Vis Sci.* 2010;51(4):2101–2108.

11. Knickelbein JE, Watkins SC, McMenamin PG, Hendricks RL. Stratification of antigen-presenting cells within the normal cornea. *Ophthalmol Eye Dis.* 2009;1:45–54.

12. Gao N, Lee P, Yu FS. Intraepithelial dendritic cells and sensory nerves are structurally associated and functional interdependent in the cornea. *Sci Rep.* 2016;6:36414.

13. Ivanusic JJ, Wood RJ, Brock JA. Sensory and sympathetic innervation of the mouse and guinea pig corneal epithelium. *J Comp Neurol.* 2013;521(4):877–893.

14. Bereiter DA, Rahman M, Thompson R, Stephenson P, Saito H. TRPV1 and TRPM8 channels and nocifensive behavior in a rat model for dry eye. *Invest Ophthalmol Vis Sci.* 2018;59(8):3739–3746.

15. Yamaguchi T, Calvacanti BM, Cruzat A, et al. Correlation between human tear cytokine levels and cellular corneal changes in patients with bacterial keratitis by in vivo confocal microscopy. *Invest Ophthalmol Vis Sci.* 2014;55(11):7457–7466.

16. Cavalcanti BM, Cruzat A, Sahin A, et al. In vivo confocal microscopy detects bilateral changes of corneal immune cells and nerves in unilateral herpes zoster ophthalmicus. *Ocul Surf.* 2018;16(1):101–111.

17. Xiang J, Le Q, Li Y, Xu J. In vivo confocal microscopy of early corneal epithelial recovery in patients with chemical injury. *Eye (London, England).* 2015;29(12):1570–1578.

18. Mastropasqua L, Nubile M, Lanzini M, et al. Epithelial dendritic cell distribution in normal and inflamed human

cornea: in vivo confocal microscopy study. *Am J Ophthalmol*. 2006;142(5):736–744.

19. Kamel JT, Zhang AC, Downie LE. Corneal epithelial dendritic cell response as a putative marker of neuro-inflammation in small fiber neuropathy. *Ocul Immunol Inflamm*. 2020;28(6):898–907.

20. Lagali NS, Badian RA, Liu X, et al. Dendritic cell maturation in the corneal epithelium with onset of type 2 diabetes is associated with tumor necrosis factor receptor superfamily member 9. *Sci Rep*. 2018;8(1):14248.

21. Tajbakhsh Z, Jalbert I, Kolanu S, Stapleton F, Golebiowski B. Density and morphology of corneal epithelial dendritic cells are different in allergy. *Curr Eye Res*. 2019;45(6):675–679.

22. Marsovszky L, Resch MD, Nemeth J, et al. In vivo confocal microscopic evaluation of corneal Langerhans cell density, and distribution and evaluation of dry eye in rheumatoid arthritis. *Innate Immun*. 2013;19(4):348–354.

23. Marsovszky L, Resch MD, Visontai Z, Nemeth J. Confocal microscopy of epithelial and langerhans cells of the cornea in patients using travoprost drops containing two different preservatives. *Pathol Oncol Res*. 2014;20(3):741–746.

24. He J, Ogawa Y, Mukai S, et al. In vivo confocal microscopy evaluation of ocular surface with graft-versus-host disease-related dry eye disease. *Sci Rep*. 2017;7(1):10720.

25. Kheirkhah A, Qazi Y, Arnoldner MA, Suri K, Dana R. In vivo confocal microscopy in dry eye disease associated with chronic graft-versus-host disease. *Invest Ophthalmol Vis Sci*. 2016;57(11):4686–4691.

26. Aggarwal S, Kheirkhah A, Cavalcanti BM, et al. Correlation of corneal immune cell changes with clinical severity in dry eye disease: an in vivo confocal microscopy study. *Ocul Surf*. 2020;19:183–189.

27. Kheirkhah A, Rahimi Darabad R, Cruzat A, et al. Corneal epithelial immune dendritic cell alterations in subtypes of dry eye disease: a pilot in vivo confocal microscopic study. *Invest Ophthalmol Vis Sci*. 2015;56(12):7179–7185.

28. Alcalde I, Inigo-Portugues A, Gonzalez-Gonzalez O, et al. Morphological and functional changes in TRPM8-expressing corneal cold thermoreceptor neurons during aging and their impact on tearing in mice. *J Comp Neurol*. 2018;526(11):1859–1874.

29. De Silva MEH, Hill LJ, Downie LE, Chinnery HR. The effects of aging on corneal and ocular surface homeostasis in mice. *Invest Ophthalmol Vis Sci*. 2019;60(7):2705–2715.

30. Jiao H, Naranjo Golborne C, Dando SJ, et al. Topographical and morphological differences of corneal dendritic cells during steady state and inflammation. *Ocul Immunol Inflamm*. 2020;28(6):898–907.

31. Hamrah P, Zhang Q, Liu Y, Dana MR. Novel characterization of MHC class II-negative population of resident corneal Langerhans cell-type dendritic cells. *Invest Ophthalmol Vis Sci*. 2002;43(3):639–646.

32. Jiao H, Downie LE, Huang X, et al. Novel alterations in corneal neuroimmune phenotypes in mice with central nervous system tauopathy. *J Neuroinflamm*. 2020;17(1):136.

33. Knickelbein JE, Buela KA, Hendricks RL. Antigen-presenting cells are stratified within normal human corneas and are rapidly mobilized during ex vivo viral infection. *Invest Ophthalmol Vis Sci*. 2014;55(2):1118–1123.

34. Yamagami S, Yokoo S, Amano S, Ebihara N. Characterization of bone marrow–derived cells in the substantia propria of the human conjunctiva. *Invest Ophthalmol Vis Sci*. 2007;48(10):4476–4481.

35. Hazlett LD, McClellan S, Barrett R, Rudner X. B7/CD28 costimulation is critical in susceptibility to Pseudomonas aeruginosa corneal infection: a comparative study using monoclonal antibody blockade and CD28-deficient mice. *J Immunol (Baltimore, MD : 1950)*. 2001;166(2):1292–1299.

36. Chen W, Lin H, Dong N, et al. Cauterization of central cornea induces recruitment of major histocompatibility complex class II+ Langerhans cells from limbal basal epithelium. *Cornea*. 2010;29(1):73–79.

37. Chessa F, Mathow D, Wang S, et al. The renal microenvironment modifies dendritic cell phenotype. *Kidney Intl*. 2016;89(1):82–94.

38. Popovic ZV, Embgenbroich M, Chessa F, et al. Hyperosmolarity impedes the cross-priming competence of dendritic cells in a TRIF-dependent manner. *Sci Rep*. 2017;7(1):311.

39. Cope EC, LaMarca EA, Monari PK, et al. Microglia play an active role in obesity-associated cognitive decline. *J Neurosci : the Official J Soc Neurosci*. 2018;38(41):8889–8904.

40. Mayer WJ, Irschick UM, Moser P, et al. Characterization of antigen-presenting cells in fresh and cultured human corneas using novel dendritic cell markers. *Invest Ophthalmol Vis Sci*. 2007;48(10):4459–4467.

41. Wu M, Downie LE, Grover LM, et al. The neuroregenerative effects of topical decorin on the injured mouse cornea. *J Neuroinflamm*. 2020;17(1):142–142.

42. Alzahrani Y, Colorado LH, Pritchard N, Efron N. Longitudinal changes in Langerhans cell density of the cornea and conjunctiva in contact lens-induced dry eye. *Clin Exp Optom*. 2017;100(1):33–40.

43. Whiteside G, Munglani R. TUNEL, Hoechst and immunohistochemistry triple-labelling: an improved method for detection of apoptosis in tissue sections—an update. *Brain Res Brain Res Protoc*. 1998;3(1):52–53.

44. Willcox MDP, Argueso P, Georgiev GA, et al. TFOS DEWS II Tear Film Report. *Ocul Surf*. 2017;15(3):366–403.

45. Maruoka S, Inaba M, Ogata N. Activation of dendritic cells in dry eye mouse model. *Invest Ophthalmol Vis Sci*. 2018;59(8):3269–3277.

46. Jamali A, Seyed-Razavi Y, Chao C, et al. Intravital multiphoton microscopy of the ocular surface: alterations in conventional dendritic cell morphology and kinetics in dry eye disease. *Front Immunol*. 2020;11:742.

47. Ward BR, Jester JV, Nishibu A, et al. Local thermal injury elicits immediate dynamic behavioural responses by corneal Langerhans cells. *Immunology*. 2007;120(4):556–572.

48. Holst K, Guseva D, Schindler S, et al. The serotonin receptor 5-HT(7)R regulates the morphology and migratory properties of dendritic cells. *J Cell Sci*. 2015;128(15):2866–2880.

49. Lindquist RL, Shakhar G, Dudziak D, et al. Visualizing dendritic cell networks in vivo. *Nat Immunol*. 2004;5(12):1243–1250.

50. Chinnery HR, Ruitenberg MJ, Plant GW, et al. The chemokine receptor CX3CR1 mediates homing of MHC class II-positive cells to the normal mouse corneal epithelium. *Invest Ophthalmol Vis Sci*. 2007;48(4):1568–1574.

51. Seyed-Razavi Y, Lopez MJ, Mantopoulos D, et al. Kinetics of corneal leukocytes by intravital multiphoton microscopy. *FASEB J*. 2019;33(2):2199–2211.

52. Dehghani C, Frost S, Jayasena R, et al. Morphometric changes to corneal dendritic cells in individuals with mild cognitive impairment. *Front Neurosci*. 2020;14:1242.

53. Puro DG. Role of ion channels in the functional response of conjunctival goblet cells to dry eye. *Am J Physiol Cell Physiol*. 2018;315(2):C236–C246.

54. Hirata H, Mizerska K, Dallacasagrande V, Rosenblatt MI. Estimating the osmolarities of tears during evaporation through the "eyes" of the corneal nerves. *Invest Ophthalmol Vis Sci*. 2017;58(1):168–178.

55. Vega-Ramos J, Roquilly A, Zhan Y, et al. Inflammation conditions mature dendritic cells to retain the capacity to present new antigens but with altered cytokine secretion

function. *J Immunol (Baltimore, Md : 1950)*. 2014;193(8): 3851–3859.

56. Luís A, Martins JD, Silva A, et al. Oxidative stress-dependent activation of the eIF2α–ATFr unfolded protein response branch by skin sensitizer 1-fluoro-2, 4-dinitrobenzene modulates dendritic-like cell maturation and inflammatory status in a biphasic manner. *Free Radic Biol Med*. 2014;77:217–229.

57. Ren Y, Lu H, Reinach PS, et al. Hyperosmolarity-induced AQP5 upregulation promotes inflammation and cell death via JNK1/2 Activation in human corneal epithelial cells. *Sci Rep*. 2017;7(1):4727.

58. Peng CC, Cerretani C, Braun RJ, Radke CJ. Evaporation-driven instability of the precorneal tear film. *Adv Colloid Interface Sci*. 2014;206:250–264.

59. Yorek MS, Davidson EP, Poolman P, et al. Corneal sensitivity to hyperosmolar eye drops: a novel behavioral assay to assess diabetic peripheral neuropathy. *Invest Ophthalmol Vis Sci*. 2016;57(6):2412–2419.

60. Yin G, Levy N, Hoffart L. Clinical results after 5% sodium chloride treatment in post-operative corneal oedema. *J Eye Dis Disord*. 2018;3(113):2.

61. Agrahari V, Mandal A, Agrahari V, et al. A comprehensive insight on ocular pharmacokinetics. *Drug Deliv Transl Res*. 2016;6(6):735–754.

62. Ozdemir M, Temizdemir H. Age- and gender-related tear function changes in normal population. *Eye (London, England)*. 2010;24(1):79–83.

63. Su Y, Liang Q, Su G, et al. Spontaneous eye blink patterns in dry eye: clinical correlations. *Invest Ophthalmol Vis Sci*. 2018;59(12):5149–5156.

64. Portello JK, Rosenfield M, Chu CA. Blink rate, incomplete blinks and computer vision syndrome. *Optom Vis Sci*. 2013;90(5):482–487.

65. Bell BA, Bonilha VL, Hagstrom SA, et al. Prolonged ocular exposure leads to retinal lesions in mice. *Exp Eye Res*. 2019;185:107672.

66. Koehn D, Meyer KJ, Syed NA, Anderson MG. Ketamine/xylazine-induced corneal damage in mice. *PLoS One*. 2015;10(7):e0132804.

67. Zernii EY, Baksheev VE, Kabanova EI, et al. Effect of general anesthesia duration on recovery of secretion and biochemical properties of tear fluid in the post-anesthetic period. *Bull Exp Biol Med*. 2018;165(2):269–271.